Preparation and Characterization of Thermoplastic Polyurethane/Organoclay Nanocomposites by Melt Intercalation Technique: Effect of Nanoclay on Morphology, Mechanical, Thermal, and Rheological Properties

A. K. Barick, D. K. Tripathy

Rubber Technology Centre, Indian Institute of Technology, Kharagpur, West Bengal 721 302, India

Received 4 April 2009; accepted 15 August 2009
DOI 10.1002/app.31303
Published online 22 March 2010 in Wiley InterScience (www.interscience.wiley.com).

ABSTRACT: Nanocomposites based on thermoplastic polyurethane (TPU) and organically modified montmorillonite (OMMT) were prepared by melt blending. Organically modified nanoclay was added to the TPU matrix in order to study the influence of the organoclay on nanophase morphology and materials properties. The interaction between TPU matrix and nanofiller was studied by infrared spectroscopy. Morphological characterization of the nanocomposites was carried out using X-ray diffraction, transmission electron microscopy, and scanning electron microscopy techniques. The results showed that melt mixing is an effective process for dispersing OMMT throughout the TPU matrix. Nanocomposites exhibit higher mechanical and thermal properties than pristine TPU. All these properties showed an increasing trend with the increase in OMMT content. Thermogravimetric analysis revealed that incorporation of organoclay enhances the thermal stability of nanocomposites significantly. Differential scanning calorimetry was used to measure the melting point and the glass transition temperature (T_g) of soft segments, which was found to shift toward higher temperature with the inclusion of organoclays. From dynamic mechanical thermal analysis, it is seen that addition of OMMT strongly influenced the storage and loss modulus of the TPU matrix. Dynamic viscoelastic properties of the nanocomposites were explored using rubber process analyzer. J Appl Polym Sci 117: 639–654, 2010

Key words: polyurethanes; nanocomposites; organoclay; electron microscopy; structure-property relations

INTRODUCTION

There has been manifold increase in the research and developments on polymer layered silicate clay nanocomposites (PLSN) over the last several years because these composites are capable of exhibiting potentially superior properties compared to the conventional macro and microcounterparts. Numerous studies have revealed that the addition of a very low percentage of layered silicates can lead to a significant enhancement in many more properties, such as stiffness and strength,[1–3] flame retardancy,[4,5] gas barrier properties,[6] ionic conductivity,[7] electrical properties,[8] thermal stability,[9] and biodegradability.[10] Lightweight and economic competitiveness using a minimal amount of reinforcing materials are other advantages of polymer clay nanocomposites. Enhancement of above properties makes these materials suitable for a variety of applications, such as automotive, electronics, food packaging, biotechnology, biomedical, etc.

The layered silicate clays are commonly used as reinforcing filler for preparation of nanocomposites due to their low cost and natural abundance. Layered silicates, which are composed of silicon oxide (SiO_2), aluminum oxide (Al_2O_3) and magnesium oxide (MgO), are classified as montmorillonite (MMT), saponite, hectorite, vermiculite, mica, talc, and kaolinite depending on the composition, structure, and layer ratio. The MMT clay is a member of the phyllosilicate group of minerals and consists of planar layers of octahedral (O) bound to tetrahedral (T) above and below with a characteristic repeat distance (gallery spacing) between the T–O–T layers. MMT is mostly favored among the smectite class of 2 : 1 layered silicate clays for polymer nanocomposites preparation because of its high cation exchange capacity (CEC), aspect ratio, surface area, surface reactivity, and adsorptive property. The Na^+ cation in MMT $[(Na,Ca)_{0.33}(Al,Mg)_2(Si_4O_{10})(OH)_2{\cdot}nH_2O]$ is

Correspondence to: D. K. Tripathy (dkt@rtc.iitkgp.ernet.in).

Contract grant sponsor: Council of Scientific and Industrial Research (CSIR), New Delhi, India; contract grant number: 22(0410)/06/EMR-II.

substituted by ammonium or phosphonium quaternary salts as hydrophobic surfactants before processing, in order to enhance better layer separation and improve compatibility with polymer matrix. Enhancement of significant properties of nanocomposites is a measure of dispersion or exfoliation of the individual silicate platelets within the polymer matrix. Two types of morphology are generally proposed for the layered silicate nanocomposites such as intercalation and exfoliation. Intercalation is a highly organized multilayered structure where the polymer chain is interspersed between each MMT layer, which results in more separated layers. Exfoliation is the further intersection of a polymer chain deep into the interspaces of MMT layers by terminating ionic interactions between each MMT layer. The affinity of the polymer with the surface of the clay and/or with the organic surfactant of the organoclay is essential to promote favorable interactions between these species which can give rise to high levels of exfoliation.

The affinity between the polymer matrix and the organoclay is determined by the polarity of the polymer and the type of organic modifier used to form the organoclay.[11–13] Thermoplastic polyurethane (TPU) has similar functional groups as polyamide (PA) but different repeating unit structures. There are growing literatures on polyurethane nanocomposites dealing with the methods of preparation, structure of polyurethane, organoclay, and hard segment concentration on degree of clay dispersion or exfoliation, microphase morphology, hydrogen bonding, rheology, mechanical properties, thermal stability, flame retardancy, water sorption, and barrier properties.[2,6,11,14–23] There are very few reports on polyurethane nanocomposites prepared by melt processing in spite of the obvious advantages of this process.[2,12,24,25] The advantages of preparing nanocomposites by melt processing are quite significant. Melt processing is environmentally sound since no solvents are required. It shifts nanocomposite production downstream, thereby giving end-use manufacturers many degrees of freedom with regard to final product specifications (e.g., selection of polymer grade, choice of organoclay, level of reinforcement, etc.). At the same time, melt processing minimizes capital costs because of its compatibility with existing processing techniques.

The objective of this study is to explore the effect of the nanoclay on the materials properties of nanocomposites. The overall properties governed by the structure-property relations are the primary aspect of this study. Mechanical, thermal, rheological properties, and morphology characterization were used to evaluate the structure and performance of these nanocomposites.

EXPERIMENTAL PROCEDURES

Materials

Commercial medical grade aliphatic, polyether-based TPU (Tecoflex® EG 80A injection grade) selected for this work was procured from Lubrizol Advanced Materials, Thermedics™ Inc. Polymer Products, USA. Tecoflex EG 80A (around 35% of hard segments) has Shore Hardness = 72A, specific gravity = 1.04, and its constituent formulation contains methylene bis(cyclohexyl) diisocyanate (HMDI) hard segment, polytetramethylene oxide (PTMO) soft segment (molecular weight = 1000 g/mol), and chain extender 1,4-butane diol (BD). Commercial organically modified Cloisite 30B nanoclay used in this study was procured from the Southern Clay Products, Inc., USA. The Cloisite 30B is an organosilicate clay based on a natural montmorillonite having density = 1.98 g/cc, d_{001} = 18.5 Å, CEC = 0.9 meq/g with methyl bis-2-hydroxyethyltallow ammonium modifier (MT2EtOH) with the tallow composition as ~ 65% C18; ~ 30% C16; ~ 5% C14. Tetrahydrofuran (THF) solvent used was availed from Merck Specialities Private Limited, Mumbai, India.

Preparation of TPU/OMMT nanocomposites

Polymer nanocomposites based on TPU and organically modified montmorillonite (OMMT) were prepared by melt intercalation technique using a Thermo Scientific HAAKE PolyLab OS Rheomix (Thermo Electron Corporation, USA) at 185°C with a rotor speed of 100 rpm and mixing time of 6 min. Varying amount of commercially available organically modified nanoclays (1, 3, 5, 7, and 9 wt %) was added to the TPU matrix. Before mixing, nanoclay and TPU were dried in a vacuum oven at 80°C for 12 h for the evaporation of moisture content (if any in the supplied materials). TPU and its nanocomposite sheets were prepared by compression molding at 180°C and samples for mechanical testing were punched from the molded sheet according to standards. Virgin TPU sample is coded as "TPU" and TPU nanocomposite samples are designated as "TPUXB." Where "*X*" values are 1, 3, 5, 7, and 9 wt % of organoclay loaded to 100 wt % of TPU matrix. B stands for Cloisite 30B organoclay.

Characterization and measurements

Fourier transform infrared (FTIR) spectra were recorded in the range of 400–4000 cm^{-1} using Perkin-Elmer FTIR-spectrophotometer (model spectrum RX-I) with a resolution of 4 $cm^{-1.}$ About 2% solution of the neat TPU and TPU nanocomposites in THF solvent were prepared and coated on KBr disks. To remove the residual THF solvent, the disks

were placed in a vacuum oven at 70°C for 24 h. The surface morphology of all samples with different filler loading was studied using an automated scanning electron microscopy (JEOL JSM-5800 Scanning Microscope, OXFORD ISIS-300 microanalytical system, and BIO-RAD E-5200 coating unit). The film surfaces were gold coated under an argon (Ar) atmosphere at a vacuum of $\sim 10^{-2}$ Torr pressure before use for the surface morphology study. The silicon elemental mapping of samples was carried out using energy-dispersive X-ray (EDX) facility of scanning electron microscope (SEM). X-ray diffraction (XRD) was performed with a Philips PW 1710 diffractometer. The samples were scanned from 2° to 10° at a scan rate of 2°/min. The Cu Kα ($\lambda = 1.54$ Å) radiation source was operated at 40 kV and 30 mA. Wide angle X-ray diffraction (WAXD) was performed with a Philips PW 1729 X-ray generator at crystal monochromated Co Kα ($\lambda = 1.79$ Å) radiation in the angular range of 10° to 50° at a scan rate of 3°/min at a voltage of 30 kV and current of 20 mA. The *d*-spacing of the clay particles was calculated using Bragg's law ($n\lambda = 2d\sin\theta$) for different samples. The distribution of clay particles into the polymer matrix was studied using a high resolution transmission electron microscopy (JEM 2100, JEOL Limited, Tokyo, Japan) operated at an accelerated voltage of 200 keV. The samples were sectioned into ~ 100 nm thin sections at –50°C using an ultramicrotome (Ultracut R, Leica) equipped with a diamond knife. Atomic force microscopy topographic images were obtained using a NanoScope IV MultiMode scanning probe microscope (Veeco Instruments, Santa Barbara, CA) using the tapping mode with a resonant oscillating frequency of 463 kHz, with commercial Si_3N_4 integral tips at ambient pressure, room temperature, and humidity on the surfaces of the compression-molded specimens. Thermal stability and composition of nanocomposites prepared were measured by thermogravimetric analysis (TGA) (Q50 V6.1 series, TA instruments, New Castle, Delaware) from room temperature to 600°C with a scan rate of 20°C/min in nitrogen (N_2) gas atmosphere. The glass transition temperature, melting point, and crystallization temperature of nanocomposite samples were evaluated by means of differential scanning calorimeters (DSC) (Q100 V8.1 series, TA instrument, USA) in the temperature range of –100 to 300°C and scan rate of 10°C/min in a liquid nitrogen atmosphere. Dynamic mechanical properties of nanocomposites were measured using dynamic mechanical thermal analyzer (DMTA 2980 V1.7B, TA instruments, USA). The test was carried out at a frequency of 1 Hz, static force of 0.1 N, and amplitude of 10 μm in the temperature range –100 to 100°C and a scan rate 3°C/min in liquid nitrogen atmosphere. Viscoelastic properties of the samples were carried out using rubber process analyzer (RPA 2000, Alpha Technologies, Akron, OH). The test was carried out at strain and temperature of 0.98% and 145°C, respectively, with a frequency range of 0.033 to 30.833 Hz. The tensile properties of the samples were determined according to ASTM D-412-98 test procedure using dumbbell-shaped specimens with a universal testing machine (Model 4468, Instron Corporation, Canton, MA). Samples were cut to $60 \times 4 \times 2$ mm^3 size by a punch cutter. The length between the jaws was fixed to 40 mm and at least five parallel measurements were done to conclude the mean values. Tests were run at room temperature at a crosshead speed of 500 mm/min and the related modulus and strength values were determined. The tear tests of the samples were carried out using unnicked 90° angle test piece by Instron universal testing machine according to ASTM D-624-81 specification.

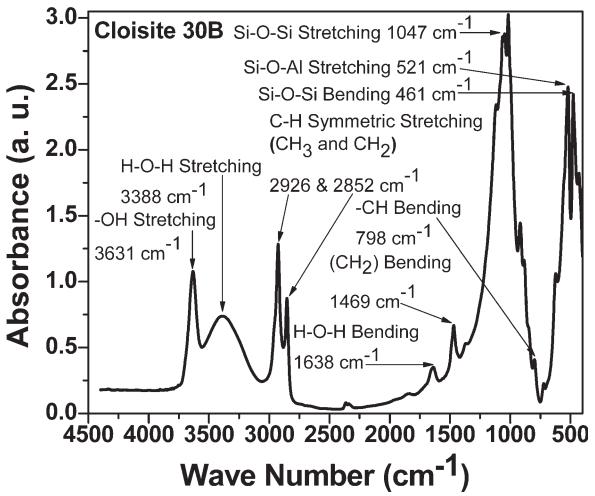

Figure 1 FTIR spectra of modified OMMT nanoclay.

RESULTS AND DISCUSSION

Fourier transform infrared spectroscopy

The FTIR spectrum of the layered silicate clay is shown in Figure 1. The FTIR spectrum shows four Si—O stretching vibration of clay at 1120, 1082, 1047, and 1018 cm^{-1} in the range of 940 to 1140 cm^{-1}. The band observed at 521 and 461 cm^{-1} can be assigned to the stretching vibration of Al—O—Si and bending mode of Si—O—Si bond, respectively.[26] Along with the above bands, FTIR spectrum also shows numerous bands, which can be associated with various group frequencies of —CH_2—, —CH, and —OH groups of the ammonium modifier present in the silicate clay as shown in Figure 1.

Further, FTIR spectra of TPU and nanocomposites were analyzed to understand the effects of clay particles on hydrogen bond formation by the hard

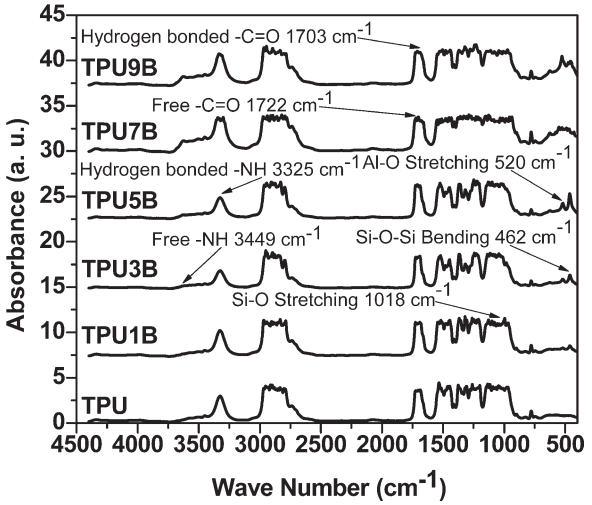

Figure 2 FTIR spectra of pure TPU and TPU/Cloisite 30B nanocomposites.

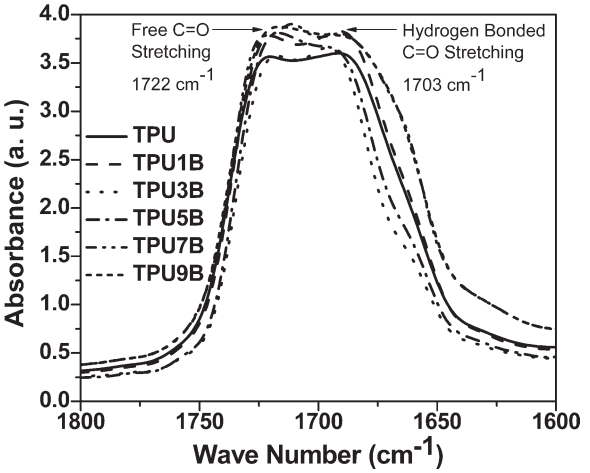

Figure 4 FTIR spectra of free and hydrogen-bonded carbonyl peaks of TPU/Cloisite 30B nanocomposites.

segments, i.e., degree of phase separation between hard and soft segments. The percentage of hydrogen-bonded >C=O group was used to define the degree of phase separation. Figure 2 represents FTIR spectra of nanocomposites prepared by melt processing from Cloisite 30B organoclays. The appeared IR bands of interest are assigned to their respective functional groups in the Figure 2.

The FTIR spectra of hydrogen-bonded —NH peaks at 3325 cm^{-1} and a small shoulder associated with stretching vibrations of free —NH groups at 3449 cm^{-1} are shown in Figure 3. From Figure 3, it is found that a majority of —NH groups in urethane linkages participated in hydrogen bonding with the >C=O group of the hard segments or with the ether linkages (—O—) of the soft segments or with the oxygen of the hydroxyl groups (—OH) in silicate layers. In case of TPU nanocomposites from Cloisite 30B,

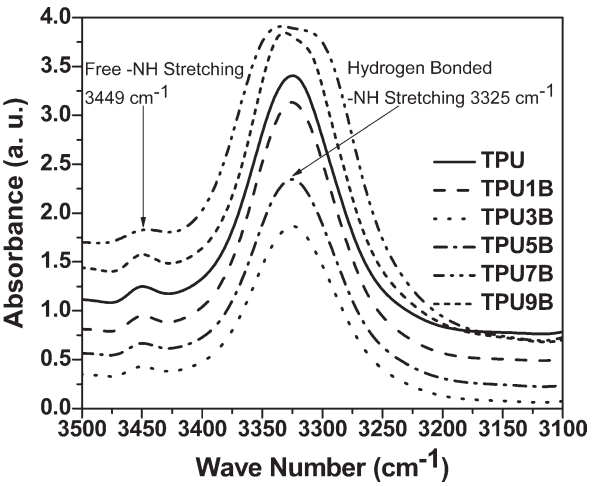

Figure 3 FTIR spectra of free and hydrogen-bonded —NH stretching region of TPU/Cloisite 30B nanocomposites.

the free and hydrogen-bonded carbonyl stretching vibration peaks appeared at around 1722 and 1703 cm^{-1} which is evident from Figure 4. This implies appreciable phase separation in case of polyether-polyol based TPU and its nanocomposites.

Table I presents the ratio of areas under various characteristic peaks and the area under the —CH peak. Theoretically, calculation of A_{NH}/A_{CH} and A_{CO}/A_{CH} ratio of virgin polymer and nanocomposites remained almost unchanged in the presence of organoclay, which indicates that clay particles did not interfere with hydrogen bond formation by urethane —NH groups. This may be due to negligible influence of hydrocarbon chains of the organic treatment of the clay to —CH stretching mode. Also the number of —CH groups present in hydrocarbon chains of organically treated clay is negligibly small compared to those derived from polyol and chain extender. It is observed that clay particles have no significant interference with hydrogen bonding among hard segments formed by urethane —NH groups with that of >C=O groups of the hard segments.

The ratio of A_{HCO}/A_{FCO} of TPU nanocomposites decreases compared to that of neat TPU as shown in Table I. This can be explained on the basis of the origin of additional hydrogen-bonded carbonyl groups in TPU nanocomposites. The hydroxyl groups in the ammonium modifier of Cloisite 30B ($—CH_2CH_2—OH$) may form hydrogen bonding with carbonyl groups in hard segment resulting in decrease in the interurethane hydrogen bonding. Some of the hydroxyls in the Cloisite 30B modifier may still form hydrogen bonding with ether oxygen in the soft segment. The hydrogen-bonded carbonyl groups can be attributed to the disturbance of phase separation of polyurethane by clay layers, which corroborate the results reported earlier in the context of

TABLE I
Ratio of the Area Under the Peak of Hydrogen-Bonded —NH (A_{NH}), Total >C=O (A_{CO}), and —CH Stretching (A_{CH}) of FTIR Spectra and the Ratio of Area Under the Peak of Hydrogen-Bonded >C=O (A_{HCO}) and Free >C=O (A_{FCO}) Groups of TPU and TPU Nanocomposites

Sample	A_{NH}/A_{CH}	A_{CO}/A_{CH}	A_{HCO}/A_{FCO}	DPS (%)	DPM (%)
TPU	0.223	0.269	1.030	50.74	49.26
TPU1B	0.219	0.281	0.948	48.66	51.33
TPU3B	0.205	0.300	0.945	48.59	51.41
TPU5B	0.218	0.296	0.940	48.45	51.54
TPU7B	0.266	0.275	0.943	48.53	51.46
TPU9B	0.269	0.278	0.941	48.48	51.51

composition and crystallinity of soft and hard segment phases.[22]

The degree of hydrogen bonding termed as hydrogen bonding index (R) is estimated by measuring the peak intensity area ratio of hydrogen bonded and free carbonyl groups (A_{HCO}/A_{FCO}). Hydrogen bonding index (R) can be obtained from a baseline approach method as following equation (1):

$$R = A_{HCO}/A_{FCO} = C_{bonded}\varepsilon_{bonded}/C_{free}\varepsilon_{free} \quad (1)$$

where C_{bonded} and C_{free} are the concentration and ε_{bonded} and ε_{free} are the extinction coefficient of hydrogen bonded and free carbonyl groups, respectively. The degree of hydrogen bonded and free phase of polyurethane called as degree of phase separation (DPS) and degree of phase mixing (DPM), respectively, can be obtained by using eqs. (2) and (3). The ratio of $\varepsilon_{bonded}/\varepsilon_{free}$ is generally considered as one.[27]

$$DPS = C_{bonded}/(C_{bonded} + C_{free}) = R/(R+1) \quad (2)$$

$$DPM = 1 - DPS \quad (3)$$

The calculated values of DPS and DPM for pure TPU and TPU/Cloisite 30B nanocomposites are given in Table I. As indicated in Table I, the phase separation ratio in neat TPU is about 50.74% and there is a significant difference in DPS and DPM between nanocomposites and TPU matrix indicating influence of the wt % of organoclay loading. This observation supports that the Cloisite 30B clay is very well dispersed throughout the TPU matrix and it appears to cover both the urethane hard segment and the soft segment polyol phase.[27]

Morphological analysis

Wide angle X-ray diffraction

The wide angle X-ray diffraction (WAXD) patterns of TPU nanocomposites are shown in Figure 5. The nanocomposites formed from Cloisite 30B organoclays have been selected for this work because of their good delaminating and dispersing properties in TPU matrix. From Figure 5, it is seen that the intense diffraction peak of Cloisite 30B nanoclay appears at $2\theta = 4.77°$ with d-spacingof $d_{001} = 18.483$ Å. But for the TPU/OMMT nanocomposites from Cloisite 30B, the WAXD peaks ($2\theta = 2°$–$10°$) almost disappeared with low amount of nanoclay loading (1, 3, and 5 wt %). It indicates that these silicate layers could be completely exfoliated and dispersed in the TPU matrix forming a nanometer scale composite. Better dispersion of the silicate layers of Cloisite 30B may be attributed to the specific interaction originating from the hydrogen bonding between carbonyl groups in TPU and hydroxyl groups in Cloisite 30B as reported in the literatures.[25] It is seen from Figure 5 that after 5 wt % nanoclay loading the XRD peak position does not change appreciably. The peak height decreases and become broader as delamination increases. The changes seen in the XRD can be explained by the fact that the polymer enters the clay galleries pushing the platelets apart and causing intercalation nanostructure. As more polymers enter the galleries, two possible changes may occur; firstly, the platelets can lose their ordered, crystalline structure, and become disordered,

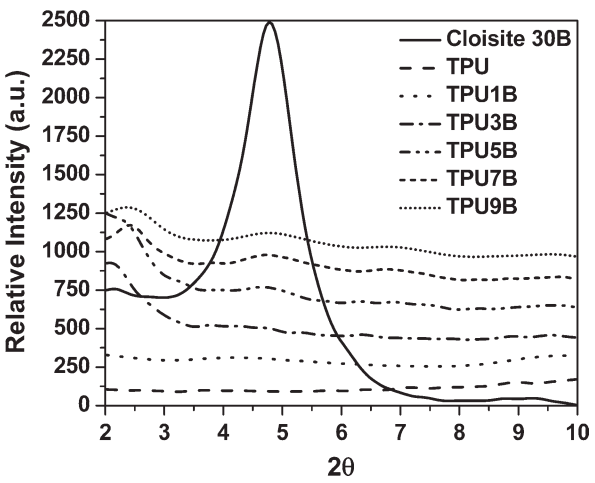

Figure 5 WAXD patterns at lower angular range of TPU/Cloisite 30B nanocomposites.

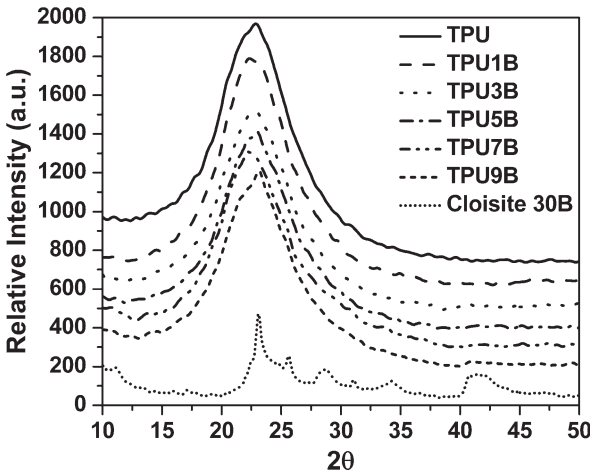

Figure 6 WAXD patterns at higher angular range of TPU/Cloisite 30B nanocomposites.

with the platelets being no longer parallel. This results in the broadening of XRD peak into the baseline formation of intercalated disordered morphology. Secondly, the polymer that enters the galleries pushes the platelets far enough apart such that the platelet separation exceeds the sensitivity of XRD leading to formation of exfoliated nanocomposites.[28]

WAXD patterns for Cloisite 30B, neat TPU, and its nanocomposites were collected in between 10° and 50° as shown in the Figure 6. WAXD pattern of Cloisite 30B display peaks assigned at 2θ values 11.1° (9.254 Å), 17.05° (6.037 Å), 23.1° (4.470 Å), 25.65° (4.032 Å), and 34.30° (3.035Å) corresponding to 002, 004, 110, 101, and 130 reflections, respectively, indicating the turbostratic stacking of layers.[29] The peak positions at 2θ values 28.75°, 31.10°, and 41.45° corresponding to *d*-spacing of 3.604, 3.338, and 2.529 Å, respectively, is due to the presence of $(Mg,Fe)SiO_3$ and $CaCO_3$ impurities in the Cloisite 30B clay.[30] However, all these peaks do not appear in case of TPU nanocomposites, either because of the homogeneous dispersion of clay in the TPU matrix breaking the clay agglomerations/tactoids or because of lower concentration of clay in the TPU matrix. It is evident

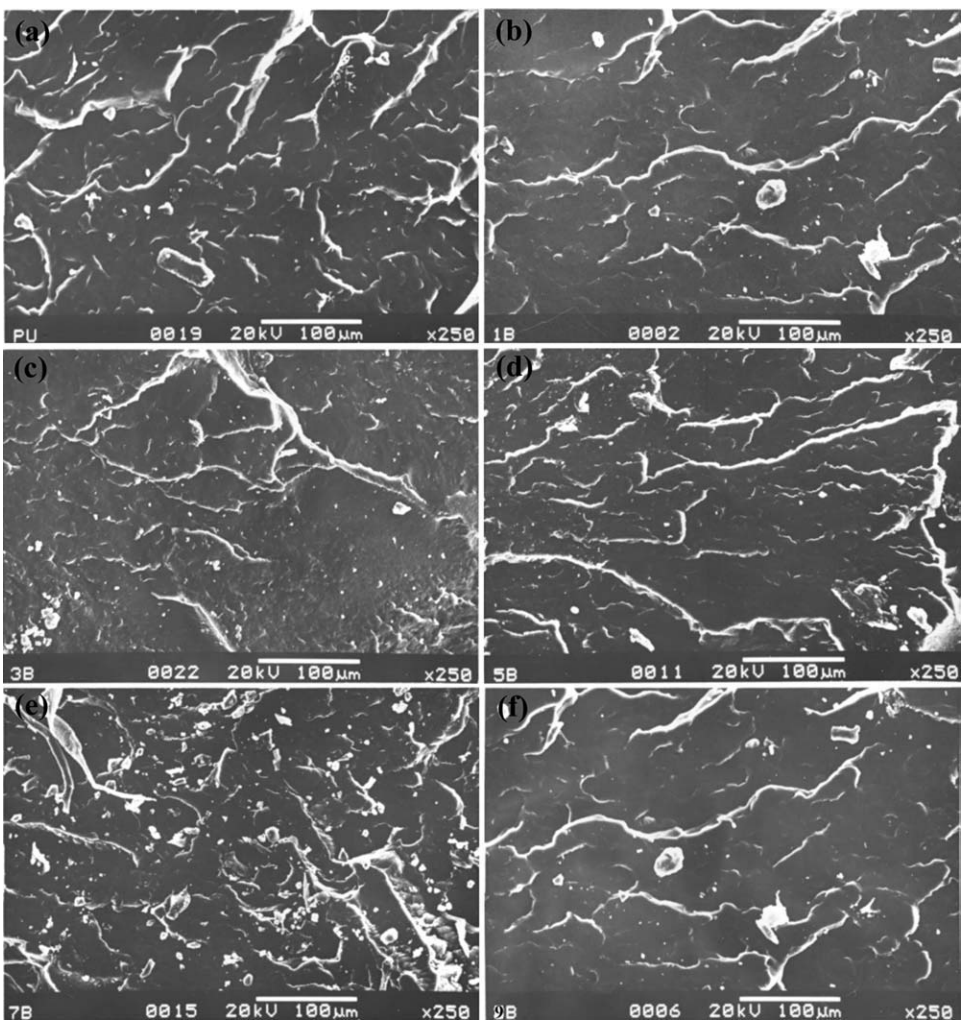

Figure 7 SEM photomicrographs of cryofractured surface of (a) Pure TPU and (b–f) TPU/Cloisite 30B nanocomposite of 1, 3, 5, 7, and 9 wt % nanoclay loading samples, respectively.

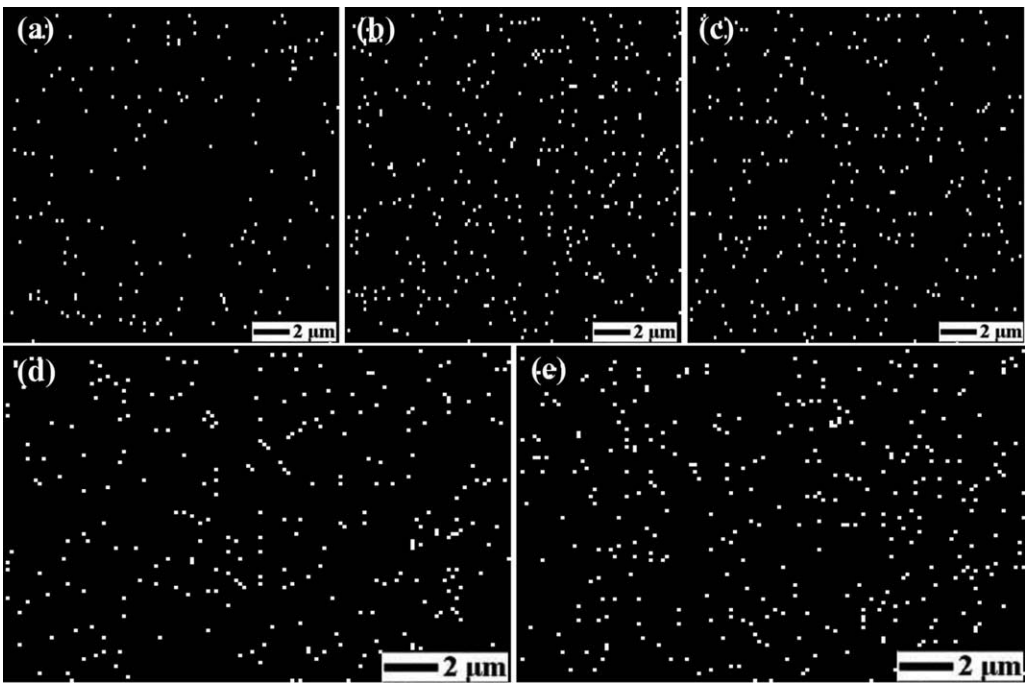

Figure 8 SEM-EDX photomicrographs of silicon dot mapping of (a–e) TPU nanocomposites with Cloisite 30B of 1, 3, 5, 7, and 9 wt % nanoclay loading samples, respectively.

that nanoclay has no influence on the amorphous structure of either hard or soft segment. The result indicates that no crystallinity structure is found in the system by WAXD analysis. Only a much diffused diffraction peak with maximum intensity at around $2\theta = 22.5^\circ$ corresponding to *d*-spacing of 4.587 Å of 110 reflections appear for all TPU nanocomposites. This broad band may be attributed to a short range ordering of hard chain segment domains, which indicates the amorphous arrangement of chain segments.[16,31]

Scanning electron microscopy

The cryogenic fractured surface of pristine TPU and its nanocomposites films containing 1 to 9 wt % organoclays were analyzed using SEM. The SEM microstructures of aggregated clay morphology of TPU nanocomposites are shown in Figure 7(a–f). The bright spots on the images correspond to clay aggregates. The clay particles are almost finely dispersed in the material. The large clay aggregates can easily be imaged in SEM, even though SEM cannot detect its finest dispersion due to the large difference in scattering density of clay and TPU. The alkyl ammonium ions render the clay organophilic and allow a better dispersion of the clay in an organic medium. Small particle aggregates are observed at relatively low magnification. This is very important in the context of mechanical properties where the microstructure rather than the nanostructure may control several phenomena.[32] Unlike pure TPU, the fractured surfaces of all nanocomposite samples showed rough surface. The coarseness of the fractured surface results in deformed portion, which may be due to agglomeration of clay particles.[6]

Energy-dispersive X-ray

The elemental mapping was performed to qualitatively confirm the presence of OMMT molecules on the surface and in the bulk of TPU nanocomposite samples using energy dispersive X-ray (EDX) facility of SEM. SEM-EDX photomicrographs of silicon dot mapping of melt pressed surface of TPU nanocomposites with different concentrations of Cloisite 30B are shown in Figure 8(a–e). SEM-EDX silicon mapping results indicate the homogeneous dispersion of the layered silicate clay in the polymer matrix. The white dots in Figure 8 correspond to the X-ray signals of SiKα lines produced from silicon elements present in the OMMT nanoparticles. SEM micrographs and differences in the silicon dot intensity observed in the EDX analysis indicate that OMMT molecules have an affinity for the surface.

Transmission electron microscopy

The state of dispersion of the clay has been investigated by transmission electron microscopy (TEM). Although XRD is the simplest method available to measure the *d*-spacing of the nanocomposites, SEM and TEM are also used for visual evaluation of the degree of intercalation/exfoliation and the amount

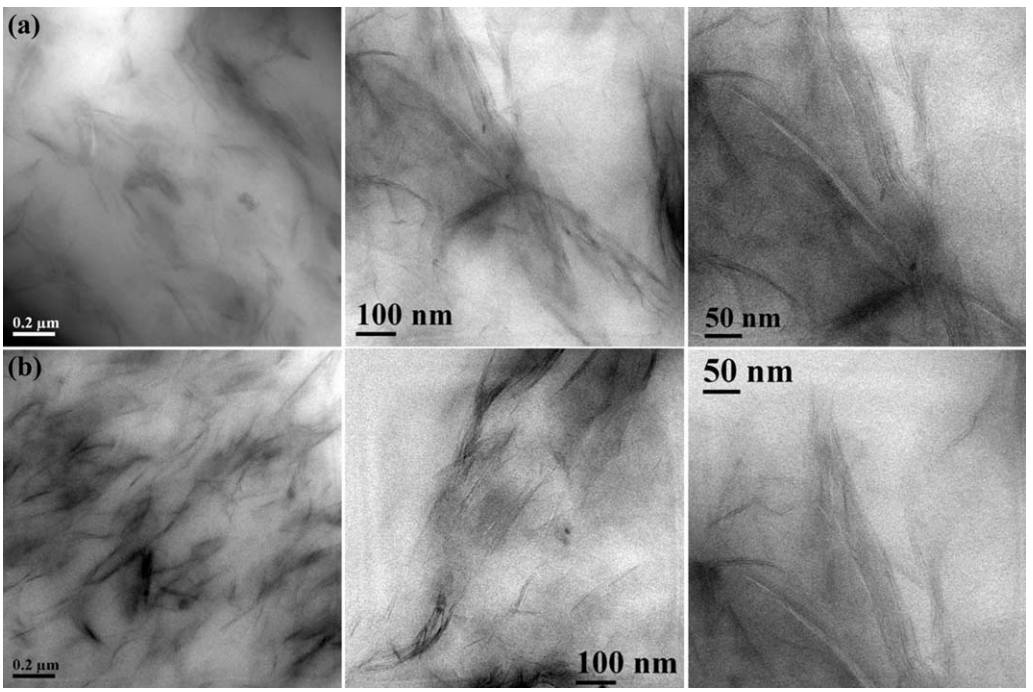

Figure 9 TEM images of TPU nanocomposites with Cloisite 30B of (a, b) 3 and 5 wt % nanoclay loading samples (left to right ×15K, ×25K, and ×40K resolutions), respectively.

of aggregation/tactoids of clay clusters. The TEM analysis not only tends to support the findings from XRD but also shows that the clay is well dispersed on the nanoscale in all compositions. The efficiency of the clay in modifying the properties of the matrix polymer is primarily determined by the degree of its dispersion in the polymer matrix. More direct evidence of the formation of a true nanocomposite is provided by TEM of an ultramicrotome cut section. The TEM microphotographs of the cross sectional views of TPU/OMMT nanocomposites containing 3 and 5 wt % organoclays loading are presented in Figure 9(a,b). The dark lines in the microphotograph are the intersections of about 1-nm-thick clay layers and the spaces between the dark lines are interlayer spaces. TEM photography shows that most clay layers are parallel to the surface of the films and are dispersed homogeneously into the polymer matrix, and small clusters of intercalated silicates and a portion of exfoliated silicates are also visible in all images. It appears that significantly good dispersion and delamination have been achieved via melt compounding. This result can be attributed to the higher shear stresses involved with the twin roller rotor. The good degree of exfoliation achieved in this system can be attributed to the strong driving force for intercalation provided by the potential for hydrogen bonding between the polymer and filler. The hydroxyl groups in Cloisite 30B are capable of forming hydrogen bonds with the hard segments and to a lesser extent with the soft segment ether oxygen. A similar arrangement of the layers can be observed in Figure 9 with the presence of one or several clay layers in the TPU matrix that indicates that nanocomposites were formed. TPU nanocomposites containing Cloisite 30B show that the clay layers are more exfoliated and dispersed randomly into the matrix polymer. At a higher content of organoclay, a complete and effective entry of TPU molecules into the organic modified silicate layers could not be

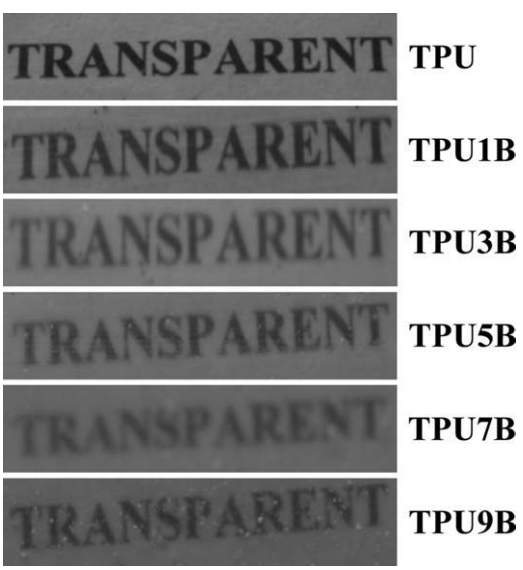

Figure 10 Optical clarity of neat TPU and TPU nanocomposites with Cloisite 30B of 1, 3, 5, 7, and 9 wt % nanoclay loading samples, respectively. In each case, a 3-mm-thick sample film was kept on a white paper with the word transparent written on it.

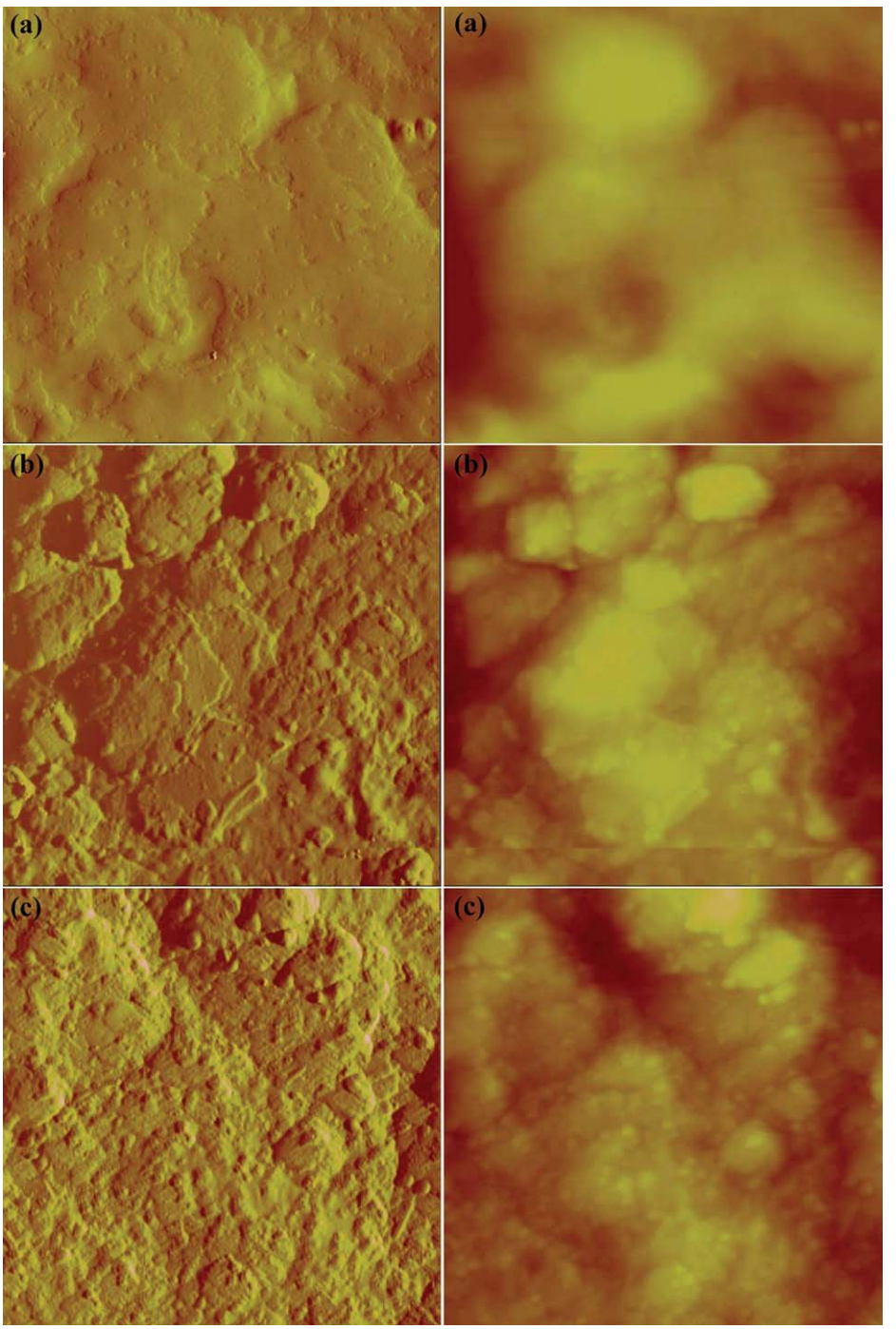

Figure 11 AFM images represent height image (right) and phase image (left) of (a) pristine TPU and (b, c) TPU nanocomposites with Cloisite 30B of 3 and 5 wt % nanoclay loading samples (5 × 5 μm^2 scan area), respectively. [Color figure can be viewed in the online issue, which is available at www.interscience.wiley.com.]

achieved to cause a thorough exfoliation of silicate layers in the TPU. It is also observed that some of the properties such as optical properties exhibited by nanoparticles are different from those obtained with the conventional composites having large particles. Figure 10 represents a visual inspection of optical clarity of 3-mm-thick neat TPU and TPU nanocomposite specimens. The thin films of nanocomposites are found to be transparent as neat TPU even with 9 wt % of organoclay as the nanoparticulates of organoclay are much smaller than the wavelength of visible light (400–800 nm).

Atomic force microscopy

AFM Study that shows the nanophase surface topography separated by hard segment domains in TPU and nanocomposites are presented in Figure 11(a–c).

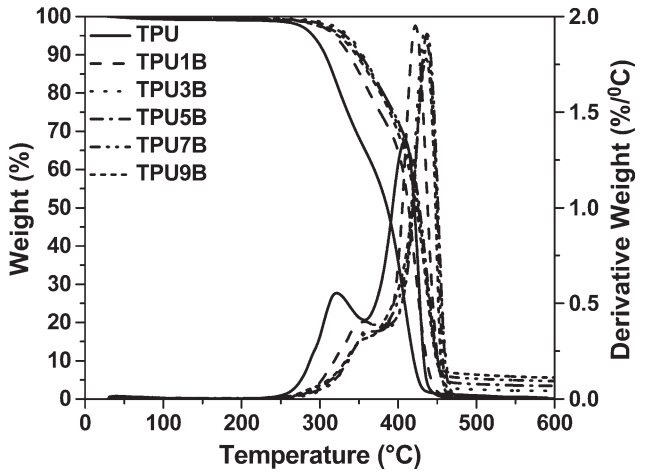

Figure 12 TGA and DTG thermograms of pure TPU and nanocomposites with Cloisite 30B samples.

It was imaged in real space using phase and topographical information from tapping-mode AFM techniques in 5 × 5 μm^2 scan surface area. AFM photograph of the surface of the TPU was very smooth whereas in case of clay nanocomposites surfaces are highly rough. Figure 11 shows nearly uniform matrix with some lighter small regions which may arises from the more elastic soft segment domains that might possess some crystallinity whereas the darker areas are indicative of more particulate hard material region. It is most likely that the soft segment, which is more elastic as compared to the hard segment, will protrude to higher elevation. In the absence of clay, the aggregates of hard domains with spherical structures of size about 800 nm have been observed. With the incorporation of clay, the size of the aggregates of hard domain is reduced to approximately 500 nm. Reduction in the size of the aggregates with the addition of clay signifies the effects of clay in the aggregation behavior of hard domains. It has been suggested elsewhere that microphase separation in TPU can produce hard microdomains, but the microdomains can approach each other and coalesce, leading to "secondary ordering."[33] The aggregation process occurs because of a strong interaction between the hard domains due to the hydrogen bonding. Also, the polyol as soft segment is a flexible long chain. However, the factors affecting the final morphology and the size of the aggregates are still not clear. Although the phase separation is severely disrupted, the sample surface is still covered with a thin layer of smooth soft phase. It seems that even this surface layer is disrupted by the addition of nanoclay in the composites.

Thermal properties

Thermogravimetric analysis

Thermal stability of the pristine TPU and its nanocomposites prepared from organically modified clay (Cloisite 30B) was carried out by thermogravimetric analysis (TGA) under nitrogen gas atmosphere as shown in Figure 12. It was found that all specimens displayed two degradation processes from room temperature to 600°C at a ramp rate of 20°C. To study the degradation thoroughly, the onset temperature (T_d) of the two degradation processes and the respective temperature of maximum degradation rate (DTG_{max}) were derived and are shown in Table II.

From the Table II, it can be seen that, compared to TPU matrix, the first onset temperature (T_{d1}) of the nanocomposites with 1 to 9 wt % of clay is found to be higher and DTG thermogram shows the first maximum degradation rate peak (DTG_{1max}). First onset temperature (T_{d2}) and second maximum degradation rate peak (DTG_{2max}) of all the nanocomposites show significant increase compared to the TPU matrix. From the Table II, it can also be seen that the nanocomposites with 5 wt % organoclay exhibit maximum peak degradation temperature ($T_{50wt\%}$) value than the other nanocomposites prepared from 1, 3, 7, 9 wt % clay, which also tally with the WAXD result. The end degradation temperature ($T_{95wt\%}$) and residue obtained at 500°C ($r_{500wt\%}$) increases with increasing clay percentage that confirms the compatibility of clay with the TPU matrix. It is reported that the first degradation process corresponds to the release of the smaller molecules or unstable side chains, which usually degrade at lower temperature. The introduction of OMMT layers can

TABLE II
Thermogravimetric Analysis (TGA) Results of TPU and Nanocomposites

Sample	DTG_{1max} (°C)	DTG_{2max} (°C)	T_{d1} (°C)	T_{d2} (°C)	$T_{50wt\%}$ (°C)	$T_{95wt\%}$ (°C)	$r_{500wt\%}$ (wt %)
TPU	321.371	408.65	297.31	356.85	386.73	425.58	0.80
TPU1B	357.03	421.83	318.76	382.32	413.29	442.29	0.91
TPU3B	365.09	434.21	336.21	382.34	426.02	456.53	2.47
TPU5B	369.59	436.66	332.76	388.42	427.20	459.79	4.28
TPU7B	359.05	436.51	327.26	372.25	425.55	536.17	5.29
TPU9B	357.5	435.81	323.09	366.20	423.27	765.15	6.35
Cloisite 30B	276.71	405.90	255.53	–	–	–	–

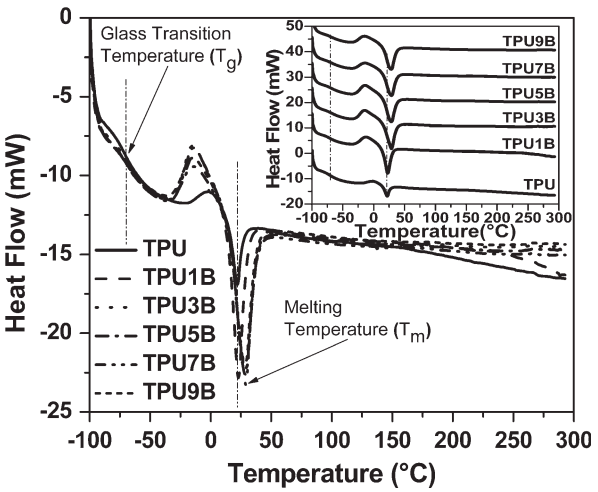

Figure 13 DSC thermograms of pure TPU and nanocomposites with Cloisite 30B samples.

greatly improve the thermal properties of the polymer matrix. The results show that the degradation rates of the nanocomposites become significantly slower compared to that of TPU, indicating improvement of thermal stability of TPU. This is because the inorganic material can prevent the heat to expand quickly and limits further degradation.[20] The thermal stabilization effect of nanoclay is explained by the so-called Labyrinth barrier effect generated by the highly anisotropic layered silicate platelets dispersed on the nanometer scale in the TPU, which hinders the diffusion of the volatile degradation products (carbon dioxide, carbon monoxide, water molecules, etc.) from the bulk of the polymer matrix to the gaseous phase.[5,34] The OMMT itself contains some smaller molecules that liberated at lower temperature; more of these molecules are likely to impair the thermal stability of the nanocomposites.[35] The degradation of the TPU molecular backbone is dominant at DTG_{2max}. The TPU nanocomposites prepared from Cloisite 30B has higher onset degradation temperature than that of the TPU, due to the extra thermal stability imposed by structure of hydroxyl group and one-alkyl groups on the quaternary ammonium modifiers. The nanocomposite derived from the one-tailed tallow organoclay has no characteristic X-ray reflections as shown in Figure 5, which suggests a highly exfoliated structure containing dispersed silicate platelets.

Differential scanning calorimetry

DSC thermograms of the pure TPU and nanocomposites are shown in Figure 13. Summary of the DSC features such as glass transition temperature ($T_{g(\text{soft})}$), soft segment melting point ($T_{m(\text{endo})}$), heat of fusion of melting (ΔH_m), percentage soft segment crystallinity ($X_{c,s}$), and change in heat capacity of soft segment at T_g(ΔC_p) are given in Table III. The structure of PU includes two segments hard and soft, which are expected to exhibit generally two melting temperatures. However, the DSC curve revealed only one peak and this endothermic peak is associated with the melting temperature of the soft segment domains. The peak associated with the melting temperature of the hard segment region is absent from the thermogram plot. This may be attributed to the inactive movement of the hard segment, which had a small heat capacity change[36] and to the widely uniform dispersion of hard segment microdomains within the TPU matrix.[37] A strong soft segment glass transition of TPU/organoclay nanocomposites is found at –70°C in all compositions. The glass transition temperature of the nanocomposites increased slightly with increasing clay content. The effect of small amounts of dispersed silicate layers on the free volume of TPU is insignificant to influence the glass transition temperature of pure TPU. This may also be attributed to the interactions between the organic and inorganic phases. These interactions enhance the rigidity of the soft segments and limit the movement of the soft segments. Therefore, the introduction of nanoparticles results in a slight increase in phase transition temperatures of the soft segments. The amorphous domain is clearly influenced by the concentration of soft and hard segments and also by the clay content.

From Table III, the change in the heat capacity associated with glass transition temperature (ΔC_p) of the nanocomposite is found to decrease as the amount of the modified clay increases from 1 to 9 wt %. The exfoliated clay layers may provide some

TABLE III
Differential Scanning Calorimetry (DSC) Results of Neat TPU and its Nanocomposites

Sample	$T_{g(\text{soft})}$ (°C)	ΔC_p (W/g)	$T_{m(\text{endo})}$ (°C)	ΔH_m (J/g)	$X_{c,s}$ (%)
TPU	−71	0.520	21.91	14.42	8.39
TPU1B	−71	0.424	22.76	36.14	21.02
TPU3B	−70	0.422	27.37	42.90	24.95
TPU5B	−70	0.389	27.80	41.87	24.60
TPU7B	−70	0.377	30.15	39.46	22.95
TPU9B	−67	0.374	29.20	39.61	23.04

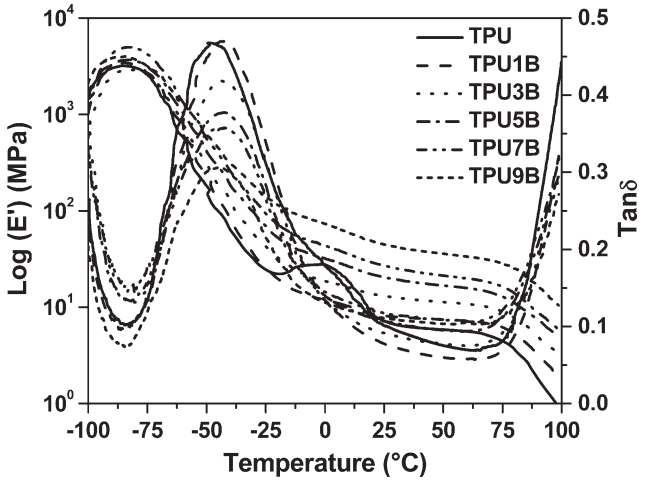

Figure 14 Storage modulus (E') and dissipation factor (tan δ) of pure TPU and TPU nanocomposites as a function of temperature.

steric hindrance to the TPU chains resulting in lowering of the ΔC_p, which may be related to the mobility of the polymer chains.[38]

The melting transition temperatures of the soft segments of pristine TPU and its nanocomposites are found to be around 22 and 30°C, respectively. It is also observed that polytetramethylene glycol (PTMG) crystallized in both neat TPU and TPU nanocomposites. This suggests that the nanoclay affects the crystal structure of the soft segments and tends to increase the melting temperature of the same with addition of organoclay due to their nucleating effect.[39] This increase in the soft segment melting temperature and enthalpy change can be attributed to the effects produced by the rigid nanoclay in the soft segment domains, leading to increasing the degree of crystallinity of the same. The value of enthalpy associated with melting in each case was also small, indicating that only small fraction of urethane linkages formed phase separated domains. Moreover, soft segment crystallinity values increased up to 5 wt % of nanoclay concentrations, beyond which it decreases. This behavior can be ascribed to the reduction in the effective surface area caused by filler platelet agglomeration at high organoclay contents.[40] Investigation into the relation between the shape memory effect and molecular structure reveals that high crystallinity of the soft segment region at room temperature is a necessary prerequisite for TPU to demonstrate shape memory behavior. The soft segment is especially important because the transition temperature of sample originates from the melting of soft segments and the corresponding crystallinity affects the shape recovery when the sample is heated above the transition temperature. As a result, the crystallinity due to the soft segments is one of the necessary conditions to show shape memory behavior that has been emphasized in this work.[41–43]

Dynamic mechanical thermal analysis

The thermomechanical behaviors of nanocomposites were assessed using dynamic mechanical thermal analysis (DMTA). The structure, concentration, and organization of the hard segments and their interaction with the soft segments have a dominant influence on the physical and mechanical properties of the urethane polymers. For this reason DMTA of the TPU nanocomposites were performed, in which the soft part contains progressively increasing clay content. The DMTA results for the determination of the glass transition of the soft-segment phase of the polyurethane are presented in Figure 14. The complete peak positions in the tan δ, storage, and loss modulus at –50 and 50°C are summarized in Table IV. The tan δ or damping factor curves of TPU nanocomposites are shown in Figure 14.

As shown in the Figure 14, the intense low temperature peak appeared in between –50 and –40°C is defined as main glass transition temperature ($T_{g(\text{soft})}$) of the system, caused due to the backbone mobilization of the amorphous soft domains. The peak at about –49°C corresponds to the glass transition temperature of the pristine TPU. For all TPU nanocomposites tan δ is shifted to a higher temperature. This shift of the tan δ peak is because of the hindered cooperative motion of the polymer chains. The value of tan δ at glass transition temperature (T_g) is also found to decrease with increasing organoclay content. This is due to the strong interfacial interaction between the matrix polymer and filler. Addition of nanoclays resulted in an increase in T_g and a reduction in

TABLE IV
Dynamic Mechanical Properties of Neat TPU and its Nanocomposites

Sample	T_g (°C)	E'_{-50} (MPa)	E'_{50} (MPa)	E''_{-50} (MPa)	E''_{50} (MPa)
TPU	−49.32	179.80	5.85	83.02	0.44
TPU1B	−41.66	229.61	7.44	103.05	0.44
TPU3B	−41.26	316.00	11.30	126.03	0.88
TPU5B	−42.46	416.70	16.78	151.40	1.60
TPU7B	−42.58	553.60	21.27	193.79	2.30
TPU9B	−44.40	623.35	35.96	187.34	3.71

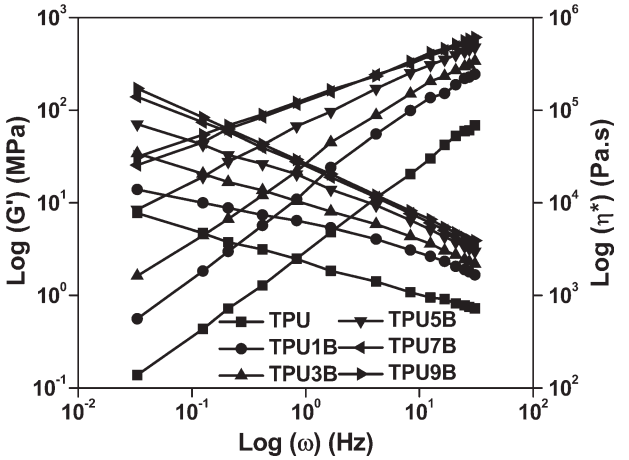

Figure 15 Storage modulus (G') and complex viscosity (η^*) of pure TPU and TPU nanocomposites as a function of frequency at 145°C and 0.98% strain.

damping capacity of TPU nanocomposites. It can be seen that the glass transition temperature is improved from –49°C of TPU matrix to around –42°C of TPU nanocomposites. This is a consequence of the well-dispersed and delaminated silicates layers restricting molecular motion. The relatively strong polymer-filler interaction present in this system, resulting from the potential for hydrogen bonding between the polymer and organoclay, is also expected to contribute to the restricted molecular motion.[2] A comparison of the storage modulus and tan δ highlights the insensitivity of the soft segment glass transition peak positions on addition of organoclay to the polyurethane matrix. However, a broadening of the peak in tan δ or breadth of segmental motion at higher temperatures is observed for the nanocomposites, which may be due to the motion of polymers at the clay–polymer matrix interface, providing evidence of reduced soft segment mobility and supporting preferential attraction of the clay particles to the highly polar soft segment.[44]

The log storage modulus (E') versus temperature curves of the TPU and nanocomposite samples are presented in Figure 14. For the pristine TPU matrix, sharp drop of elastic modulus was observed after –75°C, associated with the glass transition region of soft segment of the TPU matrix. This drop decreases the elastic modulus gradually up to –25°C. Beyond this it shows almost linear elastic behavior in between –25 and 0°C followed by a steep drop of modulus, which may be attributed to the soft segment crystallization of the polymer matrix. Finally, a gradual drop ending with the loss of mechanical consistence is observed above 75°C. Pure TPU matrix having more crystalline domains exhibits a strong modulus reduction above the soft segment melting point due to the microphase separation resulting disordering of the crystalline domains with increase in temperature. The TPU nanocomposites with 1 to 9 wt % clay loading show a higher storage modulus as compared to the pristine TPU before and after glass transition. The well dispersed and delaminated Cloisite 30B platelets restrict molecular motion resulting in an increase in storage modulus regardless of the base polymer. When the clay layers are delaminated, the exfoliated layers strongly inhibit the crystallization of TPU hard segments, i.e., the inhibiting effect of the dispersed clay layers becomes dominant than that of inducing effect which causes formation of small crystals that are disturbed at lower temperature.[13] This explanation applies to the behavior of the TPU nanocomposites from Cloisite 30B, which show steeper decreasing behavior relative to the amorphous TPU matrix.

Rheological properties

Rubber processing analyzer

Studies of rheological behavior depict an important technique for inspecting the nanoscale morphology of nanocomposites. Rubber process analyzer was used to measure the linear viscoelastic properties of pristine TPU and nanocomposites with different wt % of clay loading. The low frequency region of rheological plot reflects sensitively the effect of structure of OMMT on the viscoelastic properties of the nanocomposites. Therefore, to explore the influence of clay on the rheological behavior of the nanocomposites, the dependence modulus and complex viscosity on the frequency (ω) was studied at low frequencies. The plot of log of storage modulus (G'), loss modulus (G''), and complex viscosity (η^*) versus log of angular frequency resulting from the dynamic frequency scan measurements of TPU nanocomposites with various clay loading are shown in Figures 15 and 16, respectively.

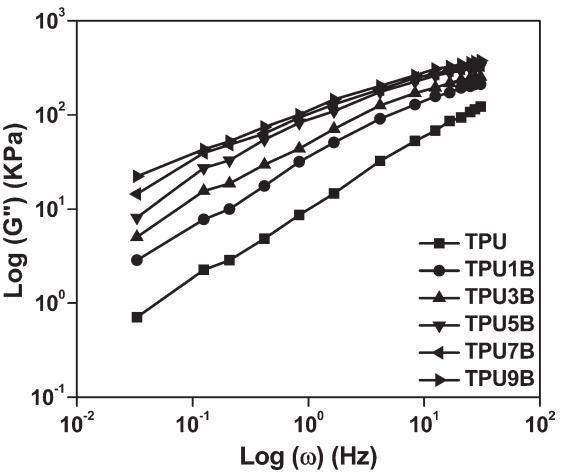

Figure 16 Loss modulus (G'') of pure TPU and TPU nanocomposites as a function of frequency at 145°C and 0.98% strain.

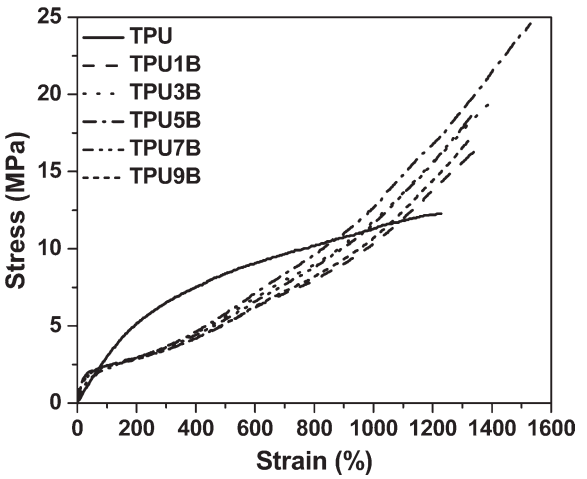

Figure 17 Tensile stress–strain diagrams of TPU and nanocomposites.

Figures 15 and 16 exhibit that the magnitude of G' and G'' monotonically increases with clay loading at low frequencies for all compositions whereas higher increase of modulus is observed at high frequency. This is because of strong filler-polymer interactions due to clay-matrix tethering, uniform nanoscale dispersion and much larger surface area of clay particles exposed to polymer chains.[21] For the range of frequency studied, the storage and loss modulus of the nanocomposite is found to be substantially higher than that of their pristine counterpart. At low frequency, the G' and G'' ranges are higher which narrows down at high frequency. This is because at low frequency, there is enough time for unraveling of the entanglements leading to a large amount of relaxation, resulting in a low value of storage and loss modulus. However, when a polymer sample is deformed at large frequency the entanglement chains do not have time to relax, so modulus goes up. The strong intramolecular attractive forces via hydrogen bonding between TPU matrix and the hydroxyl groups in the quaternary ammonium surfactant present at the surface of Cloisite 30B is also responsible for the increase of storage and loss modulus.

It is observed from Figure 15 that the complex viscosity decreases with the increase in frequency. This is due to the strong shear thinning behavior of the polymer nanocomposite and their pristine equivalent at the melted state. The substantially complex viscosity enhancement of the nanocomposite with the increase of clay content is attributed to the nanoscale dispersion of Cloisite 30B within the TPU matrix, which improves the compatibility due to strong interaction between organoclay and polymer matrix. This enhancement can be explained on the basis of resistance to flow and deformation of the molten polymer chains imposed by tethered clay particles.

Mechanical properties

Tensile properties

Tensile stress–strain curves of TPU nanocomposites containing 1 to 9 wt % OMMT are shown in Figure 17. From Figure 17, it is observed that both modulus and elongation at break of the nanocomposites increase substantially with small amount of clay loading. Detailed tensile properties of TPU nanocomposites at different compositions are also summarized in Table V. It is found that the organic-MMT content has a remarkable effect on the strength of the nanocomposites. As shown in Figure 17, the ultimate strength is found to increase dramatically with increasing organic-MMT content and reaches a maximum at 5 wt % organic-MMT content. Increase in the ultimate strength by about 152.46% for Cloisite 30B compared to pure TPU (9.74 MPa) indicates that the improved mechanical strength is dependent on the characteristics of the modifier. Such an improvement can be attributed to clay polymer tethering and hydrogen bonding between clay particles and the polymer.[22] However, the properties show a decreasing trend at high clay loading due to the filler–filler interaction and thereby reduce the contact surface between the clay and polymer matrix. The tensile modulus at 300% elongation is found to increase by about 23.32% up to clay loading of 5 wt %. This can be ascribed to high stiffness and sufficient plasticizing effect imparted by the organic surfactants used for the modification of MMT. At clay loading of 7 wt %, a decrease in the mechanical properties is observed. This may be mainly

TABLE V
Summary of Tensile and Tear Properties of Neat TPU and its Nanocomposites

Sample	Tensile strength (MPa)	Modulus, 300% elongation (MPa)	Tear strength (N/mm)	Elongation at break (%)
TPU	9.74	2.83	40.56	1228.25
TPU1B	18.54	3.10	42.50	1363.25
TPU3B	19.59	3.37	51.63	1400.75
TPU5B	24.59	3.49	54.15	1530.00
TPU7B	17.59	3.02	45.56	1329.50
TPU9B	16.67	2.93	45.17	1327.50

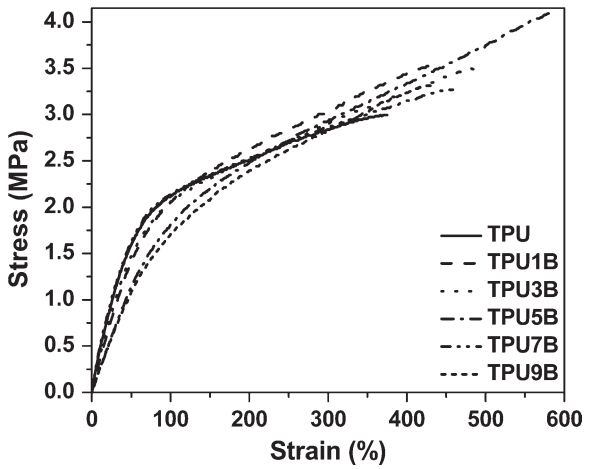

Figure 18 Tear stress versus strain diagrams of TPU and nanocomposites.

attributed to the agglomeration of organic-MMT particles above the critical content of clay.[20] The elongation behavior of nanocomposites was determined by the interfacial interaction between polyurethane and modified silicates where the gallery ammonium ions contributed to the dangling chain formation in the TPU matrix and caused a plasticizing effect in polyurethane.[45] Therefore, the maximum strength and elongation at break of polyurethane nanocomposites enhanced simultaneously.

Tear properties

Stress–strain curve for tear test of pristine TPU and its nanocomposites are shown in Figure 18. Table V shows that the tear strength of Cloisite 30B reinforced optimized TPU nanocomposites is found to increase at a tone of about 39.10% as compared to pristine TPU (38.93 N/mm). This may be due to nanometric dispersion of the silicate layers and enhancement in clay polymer interaction.

CONCLUSIONS

TPU nanocomposites were prepared successfully by melt processing technique with Cloisite 30B modified nanoclays, having good diversity of CEC, hydrophobicity, *d*-spacing, and dispersion capability. FTIR spectra indicate that Cloisite 30B nanoclay has inherent tendency to be in soft segment confinements of TPU matrix. Morphological analysis by TEM, WAXD, SEM, SEM-EDX, and AFM confirms that Cloisite clays are more prone toward the soft segment domain. WAXD studies show the formation of the exfoliated structure in case of Cloisite 30B filled nanocomposites, which exhibits no peaks corresponding to the basal spacing of OMMT. SEM and TEM studies reveal that the nanocomposite is comprised of a well dispersion of intercalated/exfoliated silicate layers throughout the matrix. SEM-EDX further confirms the homogeneous dispersion of layered silicate clays on the surface of the TPU nanocomposites. DSC thermogram shows a soft segment glass transition temperature and soft segment melting point for TPU nanocomposites. DMTA measurements illustrate that the glass transition temperature of the TPU/OMMT nanocomposite is improved from 1.0 to 8.5°C with the addition of nanoclay. TGA data reveals that TPU nanocomposites is degraded at a higher temperature because of the "Labyrinth" effect of the OMMT platelets dispersed on the nanometer scale in the TPU matrix caused by eximious barrier and strong interaction between the OMMT platelets and TPU chains. RPA results also support the homogeneous filler dispersion due to strong filler polymer interaction. Tensile and tear strength are enhanced appreciably with the incorporation of nanoclay into the TPU matrix.

One of the authors (A. K. Barick) acknowledges CSIR, India, for the award of Senior Research Fellowship (SRF). The authors thank Miku Traders, Baroda 390 005, Gujarat, India, for providing Tecoflex TPU for the research work. They thank Central Research Facility (CRF), Indian Institute of Technology, Kharagpur, for providing characterization facilities. They also thank S. Mustak for his assistance for pursuing RPA test. The helps provided by K. C. Barick, M. Nanda, R. Giri, M. Rahaman, and R. R. Babu are highly acknowledged.

References

1. Zilg, C.; Thomann, C.; Mülhaupt, R.; Finter, R. J Adv Mater 1999, 11, 49.
2. Finnigan, B.; Martin, D.; Halley, P.; Truss, R.; Campbell, K. Polymer 2004, 45, 2249.
3. Mishra, J. K.; Kim, I.; Ha, C. S. Macromol Rapid Commun 2003, 24, 671.
4. Song, L.; Hu, Y.; Tang, Y.; Zhang, R.; Chen, Z.; Fan, W. Polym Degrad Stab 2005, 87, 111.
5. Berta, M.; Lindsay, C.; Pans, G.; Camino, G. Polym Degrad Stab 2006, 91, 1179.
6. Chang, J. H.; An, Y. U. J Polym Sci Part B: Polym Phys 2002, 40, 670.
7. Nam, J. D.; Hwang, S. D.; Choi, H. R.; Lee, J. H.; Kim, K. J.; Heo, S. Smart Mater Struct 2005, 14, 87.
8. Lee, H. T.; Lin, L. H. Macromolecules 2006, 39, 6133.
9. Tien, Y. I.; Wei, K. H. J Appl Polym Sci 2002, 86, 1741.
10. Jeong, E. H.; Yang, J.; Lee, H. S.; Seo, S. W.; Baik, D. H.; Kim, J.; Youk, J. H. J Appl Polym Sci 2008, 107, 803.
11. Pattanayak, A.; Jana, S. C. Polymer 2005, 46, 5183.
12. Chavarria, F.; Paul, D. R. Polymer 2006, 47, 7760.
13. Han, B.; Cheng, A.; Ji, G.; Wu, S.; Shen, J. J Appl Polym Sci 2004, 91, 2536.
14. Tien, Y. I.; Wei, K. H. Polymer 2000, 41, 1345.
15. Tien, Y. I.; Wei, K. H. Macromolecules 2001, 34, 9045.
16. Tien, Y. I.; Wei, K. H. Polymer 2001, 42, 3213.
17. Osman, M. A.; Mittal, V.; Morbidelli, M.; Suter, U. W. Macromolecules 2003, 36, 9851.
18. Choi, W. J.; Kim, S. H.; Kim, Y. J.; Kim, S. C. Polymer 2004, 45, 6045.

19. Finnigan, B.; Martin, D.; Halley, P.; Truss, R.; Campbell, K. J Appl Polym Sci 2005, 97, 300.
20. Xiong, J.; Liu, Y.; Yang, X.; Wang, X. Polym Degrad Stab 2004, 86, 549.
21. Pattanayak, A.; Jana, S. C. Polymer 2005, 46, 3394.
22. Pattanayak, A.; Jana, S. C. Polymer 2005, 46, 3275.
23. Song, L.; Hu, Y.; Li, B.; Wang, S.; Fan, W.; Chen, Z. Int J Polym Anal Charact 2003, 8, 317.
24. Dan, C. H.; Lee, M. H.; Kim, Y. D.; Min, B. H.; Kim, J. H. Polymer 2006, 47, 6718.
25. Meng, X.; Du, X.; Wang, Z.; Bi, W.; Tang, T. Compos Sci Technol 2008, 68, 1815.
26. Zhang, X.; Xu, R.; Wu, Z.; Zhou, C. Polym Int 2003, 52, 790.
27. Dan, C. H.; Kim, Y. D.; Lee, M.; Min, B. H.; Kim, J. H. J Appl Polym Sci 2008, 108, 2128.
28. Dennis, H. R.; Hunter, D. L.; Chang, D.; Kim, S.; White, J. L.; Cho, J. W.; Paul, D. R. Polymer 2001, 42, 9513.
29. Pospíšil, M.; Čapková, P.; Máříinská, D.; Maláč, Z.; Šimoník, J. J Colloid Interface Sci 2001, 236, 127.
30. Carrado, K. A. Appl Clay Sci 2000, 17, 1.
31. Hu, J. L.; Mondal, S. Polym Int 2005, 54, 764.
32. Kornmann, X.; Lindberg, H.; Berglund, L. A. Polymer 2001, 42, 1303.
33. Kaushiva, B. D.; Wilkes, G. L. Polymer 2000, 41, 6981.
34. Cheng, A.; Wu, S.; Jiang, D.; Wu, F.; Shen, J. Colloid Polym Sci 2006, 284, 1057.
35. Han, B.; Ji, G.; Wu, S.; Shen, J. Eur Polym J 2003, 39, 1641.
36. Chen, T. K.; Chui, J. Y.; Shieh, T. S. Macromolecules 1997, 30, 5068.
37. Li, Y.; Gao, T.; Liu, J.; Linliu, K.; Desper, C. R.; Chu, B. Macromolecules 1992, 25, 7365.
38. Seo, W. J.; Sung, Y. T.; Han, S. J.; Kim, Y. H.; Ryu, O. H.; Lee, H. S.; Kim, W. N. J Appl Polym Sci 2006, 101, 2879.
39. Chen, T. K.; Tien, Y. I.; Wei, K. H. J Polym Sci Part A: Polym Chem 1999, 37, 2225.
40. Wang, C. H.; Auad, M. L.; Marcovich, N. E.; Nutt, S. J Appl Polym Sci 2008, 109, 2562.
41. Cao, F.; Jana, S. C. Polymer 2007, 48, 3790.
42. Gunes, I. S.; Cao, F.; Jana, S. C. J Polym Sci Part B: Polym Phys 2008, 46, 1437.
43. Gunes, I. S.; Cao, F.; Jana, S. C. Polymer 2008, 49, 2223.
44. Korley, L. T. J.; Liff, S. M.; Kumar, N.; Mckinley, G. H.; Hammond, P. T. Macromolecules 2006, 39, 7030.
45. Wang, Z.; Pinnavaia, T. J. Chem Mater 1998, 10, 3769.